Journal of Materials Chemistry C

ROYAL SOCIETY OF CHEMISTRY

PAPER

View Article Online
View Journal | View Issue

Cite this: J. Mater. Chem. C, 2021, 9, 15505

Sky-blue delayed fluorescence molecules based on pyridine-substituted acridone for efficient organic light-emitting diodes†

Jingwen Xu,[a] Xing Wu,[a] Jingjing Guo,[a] Zujin Zhao *[a] and Ben Zhong Tang*[abc]

Received 20th August 2021,
Accepted 7th October 2021

DOI: 10.1039/d1tc03937g

rsc.li/materials-c

In comparison with green and red OLEDs, which have been well developed with satisfactory electroluminescence (EL) performances, high-efficiency blue OLEDs still need further exploration. Herein, by reasonably strengthening the rigidity of molecules, three new sky-blue thermally activated delayed fluorescence molecules based on electron-withdrawing acridone and electron-donating acridine derivatives are designed and synthesized. Their crystal and electronic structures, thermal stabilities, electrochemical behaviors and photophysical properties are systemically investigated. The results show that these molecules have high thermal and electrochemical stabilities and exhibit aggregation-induced emission and eminent sky-blue delayed fluorescence with emission peaks at 480–502 nm and high fluorescence quantum yields of 78–94% in doped films. Their OLEDs exhibit sky-blue EL emissions with peaks at 482–492 nm, and achieve excellent external quantum efficiencies of 21.8–26.8%. These results indicate that the new sky-blue delayed fluorescence molecules hold good potential as light-emitting materials for OLEDs.

Introduction

Organic light-emitting diodes (OLEDs) are regarded as the next generation of display technology because of their various advantages such as self-luminescence, high luminance, fast response, and flexibility.[1–3] In comparison with green and red OLEDs, which have been well developed with satisfactory electroluminescence (EL) performances, high-efficiency blue OLEDs still need further exploration.[4–6] In the EL process, the holes and electrons recombine to generate singlet excitons and triplet excitons with a ratio of 1 : 3. Traditional fluorescent emitters can only utilize 25% singlet excitons for light emission, thus leading to inferior EL efficiencies.[7–9] Phosphorescent emitters can harvest both 25% singlet excitons and 75% triplet excitons, achieving theoretically 100% internal quantum efficiency.[10–12] However, the employment of nonrenewable noble metals results in high manufacturing costs, and thus limits widespread application. As the third generation of luminescent materials, purely organic thermally activated delayed fluorescence (TADF) emitters hold advantages of high exciton utilization and low cost, and thus have received considerable attention in recent decades.[13–15]

Generally, TADF emitters possess small singlet–triplet energy splittings (ΔE_{ST}s) to realize fast reverse intersystem crossing (RISC) for triplet excitons. The common strategy to obtain small ΔE_{ST}s is separating the highest occupied molecular orbitals (HOMOs) and lowest unoccupied molecular orbitals (LUMOs) of molecules, which can be achieved by connecting electron donor and acceptor moieties in a highly twisted manner.[16–18] However, the highly separated molecular frontier orbitals will lead to low fluorescence quantum yields (Φ_Fs), on account of the decreased oscillator strength.[1,19] To achieve high-performance OLEDs, it is highly favored to explore TADF emitters with small ΔE_{ST}s and high Φ_Fs simultaneously. For this consideration, enhancing the molecular rigidity to restrict the molecular motion is helpful in molecular design.[20–22]

In this work, by employing pyridine-substituted acridone as an acceptor and 9,9-dimethyl-9,10-dihydroacridine (DMAC), 9,9-diphenyl-9,10-dihydroacridine (DPAC) and 10*H*-spiro[acridine-9,9′-fluorene] (SFAC) as donors, three new TADF emitters (PDAD-DMAC, PDAD-DPAC and PDAD-SFAC) are created (Fig. 1A). The

[a] State Key Laboratory of Luminescent Materials and Devices, Guangdong Provincial Key Laboratory of Luminescence from Molecular Aggregates, South China University of Technology, Guangzhou 510640, China. E-mail: mszjzhao@scut.edu.cn
[b] Shenzhen Institute of Aggregate Science and Technology, School of Science and Engineering, The Chinese University of Hong Kong, Shenzhen 518172, Guangdong, China. E-mail: tangbenz@cuhk.edu.cn
[c] Hong Kong Branch of Chinese National Engineering Research Center for Tissue Restoration & Reconstruction, The Hong Kong University of Science and Technology, Clear Water Bay, Hong Kong, China

† Electronic supplementary information (ESI) available: Materials and instruments, characterization data, TGA and DSC thermograms, cyclic voltammograms, fluorescence and phosphorescence spectra, EL spectra, photophysical parameters and EL performance data. CCDC 2053968, 2053969 and 2053971. For ESI and crystallographic data in CIF or other electronic format see DOI: 10.1039/d1tc03937g

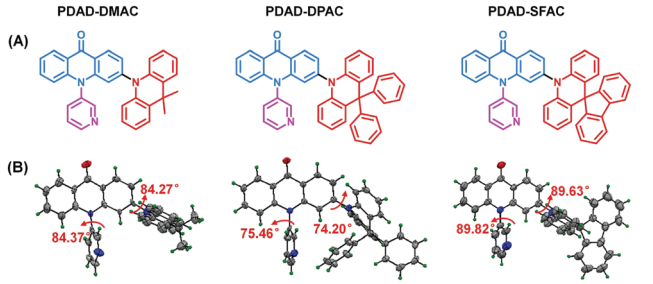

Fig. 1 (A) Molecular and (B) single-crystal structures of PDAD-DMAC, PDAD-DPAC and PDAD-SFAC.

rigid electron-withdrawing acridone is beneficial to decrease the molecular motion thus suppressing the non-radiative energy loss. Furthermore, the presence of the C=O group allows an n → π* transition, which can effectively enhance spin–orbit coupling and accelerate the RISC process.[23,24] The introduction of a pyridine moiety can strengthen the rigidity of molecules *via* intra- and/or intermolecular hydrogen bonding, which is favored for the increase of emission efficiency. Besides, the presence of a pyridine moiety at the 10 position of acridone can pose steric hindrance to the donor groups, which is conducive to maintaining large torsion angles between the acridone and donors, and is in favor of obtaining small ΔE_{ST}s. These molecules exhibit highly twisted conformations, which lead to small ΔE_{ST}s of 0.018–0.055 eV. High Φ_Fs of 78–94% are also obtained in their doped films. By employing them as emitting layers, efficient sky-blue OLEDs are fabricated with EL performance values of 59.2 cd A^{-1}, 66.4 lm W^{-1} and 26.8%.

Results and discussion

Synthesis and characterization

Scheme S1 (ESI†) illustrates the synthetic routes of the target molecules.[25] Their single crystals are obtained in tetrahydrofuran–hexane or chloroform–hexane mixtures through slow solvent evaporation, and analyzed by X-ray crystallography. As shown in Fig. 1B, these molecules adopt highly twisted conformations in crystals. The electron-withdrawing acridone core is connected with different electron-donating DMAC, DPAC and SFAC groups in a highly twisted manner, with large torsion angles of 74.20–89.63° (Fig. 1B). The almost vertical connections between donors and acceptors are in favor of the separation of molecular frontier orbitals, and facilitate the generation of small ΔE_{ST}s. On the other hand, the dihedral angles between acridone and pyridine groups also reach 75.46–89.82°. Overall, the highly distorted molecular structures are conducive to suppressing intermolecular π–π stacking that often results in decreased emission.[26–28] As displayed in Fig. S1 (ESI†), these molecules exhibit incompact molecular packing in their crystals. Owing to the existence of multiple heteroatoms, numerous weak intermolecular interactions, such as C–N···H, C=O···H and C–H···π hydrogen bonding with distances shorter than 3 Å, can be observed, which are helpful to restrict intramolecular motion, rigidify the molecular structure, and thus alleviate non-radiative decay of the molecules.[29–31]

Theoretical calculation

To depict the electric cloud distributions and energy levels of these molecules, density functional theory (DFT) calculations were carried out at the M06-2X/6-31G (d,p) level based on their crystals (Fig. 2). Because of the highly twisted molecular conformations, these molecules exhibit molecular frontier orbitals with obvious charge transfer (CT) characteristics. Taking PDAD-SFAC as an example, the HOMO and LUMO are mainly located at SFAC and acridone, respectively, with little overlap. The separated distribution of HOMO and LUMO renders a small theoretical ΔE_{ST} of 0.04 eV for PDAD-SFAC. PDAD-DMAC also has a small ΔE_{ST} of 0.02 eV, but PDAD-DPAC shows a relatively large ΔE_{ST} of 0.21 eV, which is possibly attributed to the quasi-axial conformation of PDAD-DPAC.[32–36]

Photophysical property

In tetrahydrofuran (THF) solutions, these molecules show quite similar absorption maxima at ~390 nm. The photoluminescence (PL) peak of PDAD-DMAC is located at 524 nm, which is red-shifted in comparison with those of PDAD-DPAC (503 nm) and PDAD-SFAC (508 nm), due to the stronger electron-donating ability of the DMAC moiety.[37] These molecules exhibit low Φ_Fs of 19–31% in pure THF solution (Table 1). Their PL behaviors in the aggregated state are studied by increasing the water fraction (f_w, vol%) in THF–water mixtures (Fig. 3C and Fig. S2, ESI†). At low water fractions (f_w < 80 vol%), their emissions are decreased and red-shifted with the increase of f_w, due to the intramolecular charge transfer (ICT) effect.[38] The solvatochromism properties are tested in order to confirm the ICT nature of these molecules (Fig. S3, ESI†). By enhancing the polarity of the solvent, the PL peaks of the four molecules are red-shifted evidently, verifying the ICT nature. At high water fractions (f_w ≥ 80%), these molecules form nanoaggregates, and their emissions are enhanced and blue-shifted apparently, revealing evident aggregation-induced emission (AIE) properties.[39–41] The enhanced emissions of these molecules at high f_ws can be ascribed to the suppressed intramolecular motion and weakened ICT effect in the aggregated state.[42,43]

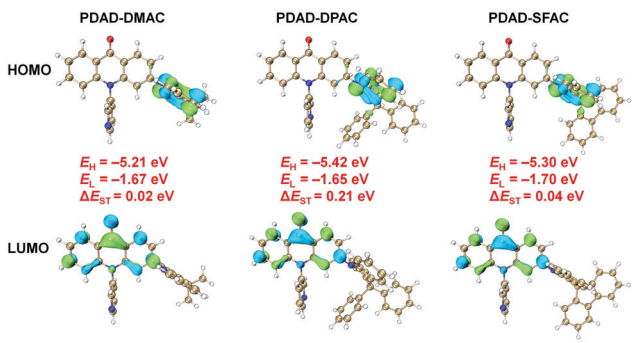

Fig. 2 Frontier orbital distributions and energy levels of PDAD-DMAC, PIPD-DPAC, and PDAD-SFAC, calculated at the M06-2X/6-31G (d,p) level, isovalue = 0.04. E_H and E_L represent the HOMO and LUMO energy levels, respectively.

Table 1 Photophysical properties of the new molecules

	Solution[a]			Doped film[b]							
Compound	λ_{abs}[c] (nm)	λ_{em}[d] (nm)	Φ_F[e] (%)	λ_{em} (nm)	Φ_F (%)	τ_{prompt}[f] (ns)	$\tau_{delayed}$[g] (μs)	Φ_{prompt}[h] (%)	$\Phi_{delayed}$[i] (%)	k_{RISC}[j] ($\times 10^5$ s^{-1})	ΔE_{ST}[k] (eV)
PDAD-DMAC	389	524	27	502	94	29.6	4.8	28.5	65.1	6.9	0.029
PDAD-DPAC	390	503	31	480	78	16.3	11.8	38.7	39.3	1.7	0.055
PDAD-SFAC	390	508	19	482	91	16.5	8.1	48.2	42.4	2.3	0.018

[a] Measured in THF solution (10^{-5} M). [b] Vacuum-deposited on a quartz substrate using PPF as the host with doping concentrations of 20, 20 and 25 wt% for PDAD-DMAC, PDAD-DPAC and PDAD-SFAC, respectively. [c] Absorption maximum. [d] Emission peak. [e] Fluorescence quantum yield determined by an integrating sphere. [f] Prompt lifetime. [g] Delayed lifetime. [h] Fluorescence quantum yield from prompt component. [i] Fluorescence quantum yield from delayed component. [j] Rate constant of RISC. [k] Singlet–triplet energy splitting, measured at 77 K.

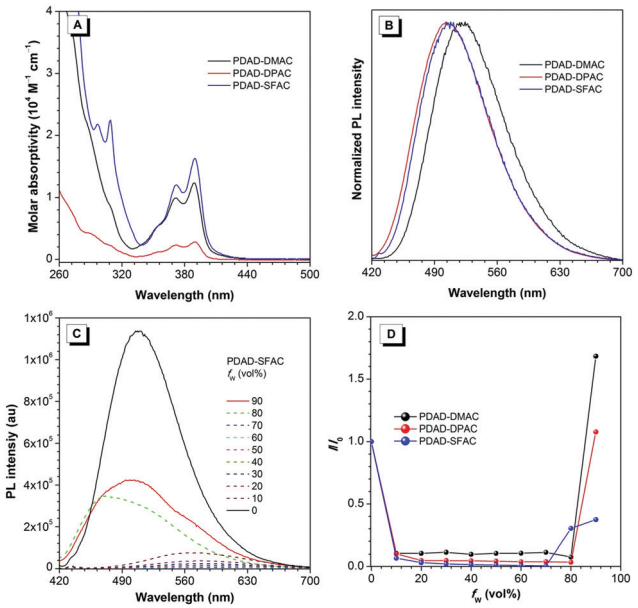

Fig. 3 (A) Absorption and (B) PL spectra of the molecules in THF solutions (10^{-5} M). (C) PL spectra of PDAD-SFAC in THF/water mixtures with different water fractions (10^{-5} M). (D) Plots of I/I_0 values *versus* water fractions (f_w). I_0 represents the PL intensity in pure THF (10^{-5} M).

These molecules were further doped into a 2,8-bis(diphenylphosphoryl)dibenzo[*b*,*d*]furan (PPF) host at concentrations of 20 wt% for PDAD-DMAC, 20 wt% for PDAD-DPAC and 25 wt% for PDAD-SFAC, and the PL properties were investigated. Compared with THF solutions, their doped films show blue-shifted PL peaks at 502, 480 and 482 nm (Fig. 4A) and higher Φ_Fs of 94%, 78% and 91% for PDAD-DMAC, PDAD-DPAC and PDAD-SFAC, respectively, which can be attributed to the rigidified molecular structures and decreased polarity of the matrix. Low temperature fluorescence and phosphorescence spectra of these molecules in doped films are collected at 77 K in order to estimate their S_1 and T_1 energy levels (Fig. S4, ESI†). The experimental ΔE_{ST} values of PDAD-DMAC and PDAD-SFAC in doped films are 0.029 and 0.018 eV, respectively, which are very close to the theoretical calculation results (0.02 and 0.04 eV). However, the experimental ΔE_{ST} value of PDAD-DPAC (0.055 eV) is much smaller than that of the theoretical value (0.21 eV). This is probably due to the conformational change from the quasi-axial conformation in the gas phase to the quasi-equatorial one in the film state. In the quasi-axial conformation, PDAD-DPAC has a relatively large ΔE_{ST}, but in the quasi-equatorial conformation, the ΔE_{ST} is greatly decreased.[44,45] As measured by transient PL decay spectra, these molecules show distinct bi-exponential decay curves, and along with the increase of temperature, the delayed components are increased clearly, revealing their typical TADF characteristics (Fig. 4B and C and Fig. S5, ESI†). The prompt lifetimes (τ_{prompt}) and delayed lifetimes ($\tau_{delayed}$) of their doped films are 16.3–29.6 ns and 4.8–11.8 μs, respectively. The RISC rate constants (k_{RISC}s) are estimated as 1.7×10^5–6.9×10^5 s^{-1} for these molecules. In comparison with PDAD-DMAC and PDAD-SFAC, PDAD-DPAC exhibits a longer $\tau_{delayed}$ and a slower k_{RISC}, probably due to its comparatively large ΔE_{ST}.

Thermal stability and electrochemical behavior

The thermal stabilities of these molecules are studied by thermogravimetric analysis (Fig. S6A, ESI†). These molecules exhibit satisfactory thermal stability with high decomposition temperatures (T_ds, 5% loss of original weight) of 368–446 °C. The high T_ds suggest that they can keep stable structures in vacuum evaporation. The electrochemical behaviors of these molecules are measured by cyclic voltammetry (Fig. S6B, ESI†). According to the onset oxidation potentials (E^{ox}_{onset}) and corresponding ferrocene potentials, the HOMO energy levels of PDAD-DMAC, PDAD-DPAC and PDAD-SFAC are calculated to be −5.27, −5.42 and −5.40 eV, respectively (HOMO = $-[E^{ox}_{onset} - E^{ox}_{Fc/Fc+} + 4.8]$ eV).[46] The LUMO energy levels are calculated as −2.71, −2.74 and −2.74 eV for PDAD-DMAC, PDAD-DPAC and PDAD-SFAC, respectively, from onset reduction potentials (E^{re}_{onset}) (LUMO = $-[E^{re}_{onset} - E^{re}_{Fc/Fc+} + 4.8]$ eV).

Electroluminescence

Inspired by the excellent photophysical properties of these molecules, their electroluminescence (EL) performances are evaluated in multilayer OLEDs with their doped films in the configuration of ITO/HATCN (5 nm)/TAPC (50 nm)/TcTa (5 nm)/mCP (5 nm)/EML (20 nm)/PPF (5 nm)/TmPyPB (30 nm)/LiF (1 nm)/Al. As shown in Fig. 5, indium tin oxide (ITO) is used as the anode, and dipyrazino[2,3-*f*:2′,3′-*h*]quinoxaline-2,3,6,7,10,11-hexacarbonitrile (HATCN), 1,1′-bis(di-4-tolylaminophenyl) cyclohexane (TAPC), 4,4′,4″-tris(carbazol-9-yl)-triphenylamine (TcTa) and *N*,*N*-dicarbazolyl-3,5-benzene (mCP) are employed as the hole-injecting layer,

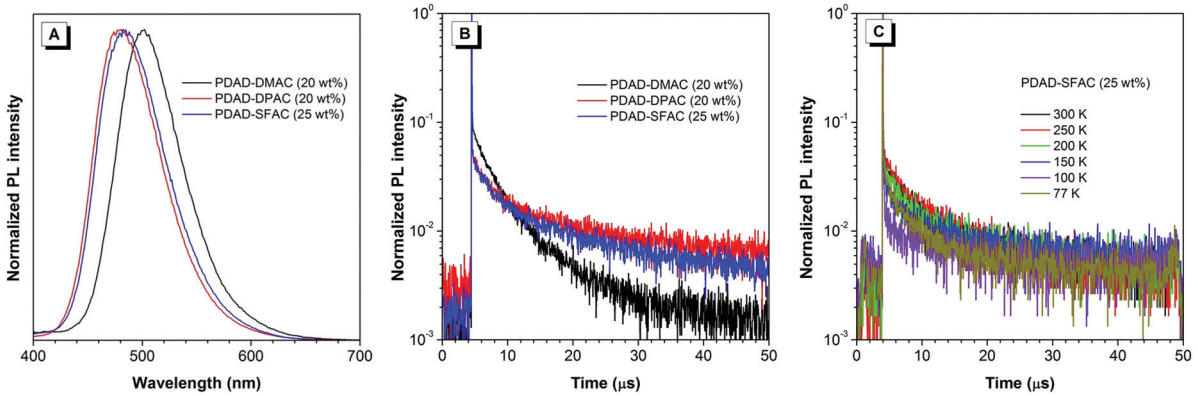

Fig. 4 (A) PL spectra of the molecules doped in the PPF host. (B) Transient PL decay spectra of the molecules in doped films, measured under nitrogen at 300 K. (C) Temperature-dependent transient PL decay spectra of PDAD-SFAC in doped film.

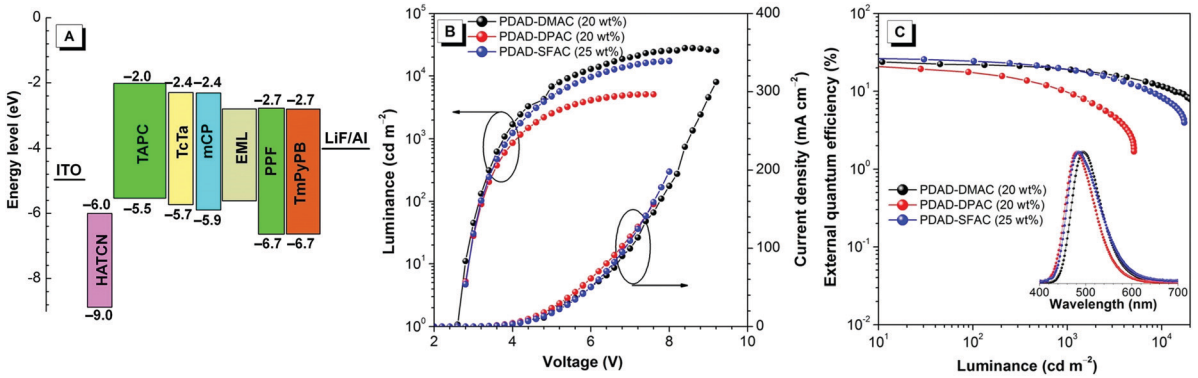

Fig. 5 (A) Device configuration and energy level diagrams. Plots of (B) luminance–voltage–current density and (C) external quantum efficiency–luminance of doped OLEDs based on the new molecules (inset in plane C: EL spectra).

Table 2 EL performances of the new molecules[a]

Emitter	V_{on} (V)	L_{max} (cd m^{-2})	$\eta_{C,max}$ (cd A^{-1})	$\eta_{P,max}$ (lm W^{-1})	$\eta_{ext,max}$ (%)	CIE (x, y)	λ_{EL} (nm)	FWHM (nm)
PDAD-DMAC	2.6	28020	60.0	72.6	24.1	(0.186, 0.461)	492	74
PDAD-DPAC	2.7	5100	42.1	47.3	21.8	(0.155, 0.321)	482	74
PDAD-SFAC	2.7	17393	59.2	66.4	26.8	(0.181, 0.386)	484	79

[a] Abbreviation: V_{on} = turn on voltage at 1 cd m^{-2}; L_{max} = maximum luminance; $\eta_{C,max}$ = maximum current efficiency; $\eta_{P,max}$ = maximum power efficiency; $\eta_{ext,max}$ = maximum external quantum efficiency; CIE = Commission Internationale de l'Eclairage coordinates; λ_{EL} = EL peak; FWHM = full width at half maximum. Device configuration: ITO/HATCN (5 nm)/TAPC (50 nm)/TcTa (5 nm)/mCP (5 nm)/EML (20 nm)/PPF (5 nm)/TmPyPB (30 nm)/LiF (1 nm)/Al, where EML represents PPF: PDAD-DMAC (20 wt%), PPF: PDAD-DPAC (20 wt%) or PPF: PDAD-SFAC (25 wt%).

hole-transporting layer, electron-blocking layer and exciton-blocking layer, respectively.[47–49] EML represents emitting layers of the doped films of these molecules in the PPF host at doping concentrations of 20 wt% or 25 wt%. PPF and 1,3,5-tri(mpyrid-3-yl-phenyl)benzene (TmPyPB) serve as the hole-blocking layer and electron-transporting layer, respectively. Thanks to the well-matched energy levels between EML and different functional layers, these devices can be turned on at low voltages of 2.6–2.7 V (Table 2). Under electrical excitation, PDAD-DMAC, PDAD-DPAC and PDAD-SFAC show sky-blue EL emissions with peaks at 492 nm (CIE$_{x,y}$ = 0.186, 0.461), 482 nm (CIE$_{x,y}$ = 0.155, 0.321) and 484 nm (CIE$_{x,y}$ = 0.181, 0.386), respectively, which are basically in good agreement with the PL emissions in doped films. In addition, because of the rigid molecular skeleton, the full width at half maximum (FWHM) values for the EL emissions from these devices are in the range of 74–79 nm, relatively narrower than those of many TADF emitters.[50] Owing to the high Φ_Fs and fast RISC processes, the OLEDs based on these molecules achieve excellent EL performances, with maximum external quantum efficiencies ($\eta_{ext,max}$s) exceeding 20%. For the devices of PDAD-DMAC and PDAD-DPAC, the $\eta_{ext,max}$s reach 24.1 and 21.8%, respectively. Among these molecules, PDAD-SFAC exhibits the best EL

properties. At a low doping concentration of 15 wt%, PDAD-SFAC shows the bluest EL peak at 476 nm ($CIE_{x,y}$ = 0.169, 0.337), and the $\eta_{ext,max}$ attains 25.3% (Fig. S7 and Table S1, ESI†). Moreover, the EL efficiencies rise with the increase of doping concentration from 15 wt% to 25 wt%. This phenomenon is probably caused by more complete energy transfer from the host to dopant.[36,51] The maximum current efficiency ($\eta_{C,max}$), maximum power efficiency ($\eta_{P,max}$) and $\eta_{ext,max}$ reach 59.2 cd A^{-1}, 66.4 lm W^{-1} and 26.8% at a doping concentration of 25 wt%.

Conclusions

In summary, three sky-blue luminescent molecules with an acridone acceptor and DMAC, DPAC and SFAC donors are designed and synthesized. These molecules show satisfactory thermal and electrochemical stabilities. Their crystals exhibit highly twisted conformations, which lead to separated HOMOs and LUMOs and thus small ΔE_{ST}s of only 0.018–0.055 eV. They have AIE and TADF properties with high Φ_Fs of 78–94% in doped films. By employing these molecules as emitters, the doped OLEDs exhibit sky-blue emission with peaks in the range of 482–492 nm, as well as excellent EL efficiencies of 21.8–26.8%, demonstrating that they are promising candidates for sky-blue OLEDs.

Conflicts of interest

The authors declare no competing financial interest.

Acknowledgements

This study was financially supported by the National Natural Science Foundation of China (21788102), the Natural Science Foundation of Guangdong Province (2019B030301003), the Innovation and Technology Commission (ITC-CNERC14SC01) and the Fundamental Research Funds for the Central Universities.

References

1 Y. Im, M. Kim, Y. J. Cho, J.-A. Seo and K. S. Yook, *Chem. Mater.*, 2017, **29**, 1946–1963.
2 Z. Yang, Z. Mao, Z. Xie, Y. Zhang, S. Liu, J. Zhao, J. Xu, Z. Chi and M. P. Aldred, *Chem. Soc. Rev.*, 2017, **46**, 915–1016.
3 J.-M. Teng, Y.-F. Wang and C.-F. Chen, *J. Mater. Chem. C*, 2020, **8**, 11340–11353.
4 Y. Tao, K. Yuan, T. Chen, P. Xu, H. Li, R. Chen, C. Zheng, L. Zhang and W. Huang, *Adv. Mater.*, 2014, **26**, 7931–7958.
5 X. Cai and S.-J. Su, *Adv. Funct. Mater.*, 2018, **28**, 1802558.
6 J.-H. Lee, C.-H. Chen, P.-H. Lee, H.-Y. Lin, M.-K. Leung, T.-L. Chiu and C.-F. Lin, *J. Mater. Chem. C*, 2019, **7**, 5874–5888.
7 Z. Xu, B. Z. Tang, Y. Wang and D. Ma, *J. Mater. Chem. C*, 2020, **8**, 2614–2642.
8 B. Chen, B. Liu, J. Zeng, H. Nie, Y. Xiong, J. Zou, H. Ning, Z. Wang, Z. Zhao and B. Z. Tang, *Adv. Funct. Mater.*, 2018, **28**, 1803369.
9 H. Nakanotani, T. Higuchi, T. Furukawa, K. Masui, K. Morimoto, M. Numata, H. Tanaka, Y. Sagara, T. Yasuda and C. Adachi, *Nat. Commun.*, 2014, **5**, 1–7.
10 C.-H. Lee, M.-C. Tang, Y.-C. Wong, M.-Y. Chan and V. W.-W. Yam, *J. Am. Chem. Soc.*, 2017, **139**, 10539–10550.
11 M.-C. Tang, W.-K. Kwok, S.-L. Lai, W.-L. Cheung, M.-Y. Chan and V. W.-W. Yam, *Chem. Sci.*, 2019, **10**, 594–605.
12 X. Li, J. Zhang, Z. Zhao, L. Wang, H. Yang, Q. Chang, N. Jiang, Z. Liu, Z. Bian, W. Liu, Z. Lu and C. Huang, *Adv. Mater.*, 2018, **30**, 1705005.
13 T. Huang, W. Jiang and L. Duan, *J. Mater. Chem. C*, 2018, **6**, 5577–5596.
14 S. K. Jeon, H. L. Lee, K. S. Yook and J. Y. Lee, *Adv. Mater.*, 2019, **31**, 1803524.
15 M. Godumala, S. Choi, M. J. Cho and D. H. Choi, *J. Mater. Chem. C*, 2019, **7**, 2172–2198.
16 X. Lv, R. Huang, S. Sun, Q. Zhang, S. Xiang, S. Ye, P. Leng, F. B. Dias and L. Wang, *ACS Appl. Mater. Interfaces*, 2019, **11**, 10758–10767.
17 P. L. d. Santos, D. Chen, P. Rajamalli, T. Matulaitis, D. B. Cordes, A. M. Z. Slawin, D. Jacquemin, E. Zysman-Colman and I. D. W. Samuel, *ACS Appl. Mater. Interfaces*, 2019, **11**, 45171–45179.
18 M. Godumala, S. Choi, M. J. Cho and D. H. Choi, *J. Mater. Chem. C*, 2016, **4**, 11355–11381.
19 L. Yu, Z. Wu, G. Xie, C. Zhong, Z. Zhu, D. Ma and C. Yang, *Chem. Commun.*, 2018, **54**, 1379–1382.
20 Y. H. Lee, S. Park, J. Oh, J. W. Shin, J. Jung, S. Yoo and M. H. Lee, *ACS Appl. Mater. Interfaces*, 2017, **9**, 24035–24042.
21 P. Rajamalli, N. Senthilkumar, P. Y. Huang, C. C. Ren-Wu, H. W. Lin and C. H. Cheng, *J. Am. Chem. Soc.*, 2017, **139**, 10948–10951.
22 F. Ma, Y. Cheng, X. Zhang, X. Gu, Y. Zheng, K. Hasrat and Z. Qi, *Dyes Pigm.*, 2019, **166**, 245–253.
23 Z. Chen, F. Ni, Z. Wu, Y. Hou, C. Zhong, M. Huang, G. Xie, D. Ma and C. Yang, *J. Phys. Chem. Lett.*, 2019, **10**, 2669–2675.
24 J. Huang, H. Nie, J. Zeng, Z. Zhuang, S. Gan, Y. Cai, J. Guo, S.-J. Su, Z. Zhao and B. Z. Tang, *Angew. Chem., Int. Ed.*, 2017, **56**, 12971–12976.
25 J. Zeng, J. Guo, H. Liu, Z. Zhao and B. Z. Tang, *Adv. Funct. Mater.*, 2020, **30**, 2000019.
26 H. Liu, J. Zeng, J. Guo, H. Nie, Z. Zhao and B. Z. Tang, *Angew. Chem., Int. Ed.*, 2018, **57**, 9290–9294.
27 Z. Huang, Z. Bin, R. Su, F. Yang, J. Lan and J. You, *Angew. Chem., Int. Ed.*, 2020, **59**, 9992–9996.
28 S. Chen, P. Zeng, W. Wang, X. Wang, Y. Wu, P. Lin and Z. Peng, *J. Mater. Chem. C*, 2019, **7**, 2886–2897.
29 F. Ma, G. Zhao, Y. Zheng, F. He, K. Hasrat and Z. Qi, *ACS Appl. Mater. Interfaces*, 2019, **12**, 1179–1189.
30 Q. Zhang, S. Sun, W. Liu, P. Leng, X. Lv, Y. Wang, H. Chen, S. Ye, S. Zhuang and L. Wang, *J. Mater. Chem. C*, 2019, **7**, 9487–9495.

31 S. Xiang, Z. Huang, S. Sun, X. Lv, L. Fan, S. Ye, H. Chen, R. Guo and L. Wang, *J. Mater. Chem. C*, 2018, **6**, 11436–11443.
32 C. Li, J. Liang, B. Liang, Z. Li, Z. Cheng, G. Yang and Y. Wang, *Adv. Opt. Mater.*, 2019, **7**, 1801667.
33 H. Tanaka, K. Shizu, H. Nakanotani and C. Adachi, *J. Phys. Chem. C*, 2014, **118**, 15985–15994.
34 M. Okazaki, Y. Takeda, P. Data, P. Pander, H. Higginbotham, A. P. Monkman and S. Minakata, *Chem. Sci.*, 2017, **8**, 2677–2686.
35 J. Yang, J. Qin, P. Geng, J. Wang, M. Fang and Z. Li, *Angew. Chem., Int. Ed.*, 2018, **57**, 14174–14178.
36 S. Xiang, R. Guo, Z. Huang, X. Lv, S. Sun, H. Chen, Q. Zhang and L. Wang, *Dyes Pigm.*, 2019, **170**, 107636.
37 Y. Wang, J. H. Yun, L. Wang and J. Y. Lee, *Adv. Funct. Mater.*, 2021, **31**, 2008332.
38 S. Gan, S. Hu, X.-L. Li, J. Zeng, D. Zhang, T. Huang, W. Luo, Z. Zhao, L. Duan, S.-J. Su and B. Z. Tang, *ACS Appl. Mater. Interfaces*, 2018, **10**, 17327–17334.
39 Y. Hong, J. W. Lam and B. Z. Tang, *Chem. Soc. Rev.*, 2011, **40**, 5361–5388.
40 J. Mei, N. L. Leung, R. T. Kwok, J. W. Lam and B. Z. Tang, *Chem. Rev.*, 2015, **115**, 11718–11940.
41 Z. Zhao, H. Zhang, J. W. Lam and B. Z. Tang, *Angew. Chem., Int. Ed.*, 2020, **59**, 9888–9907.
42 J. Guo, Z. Zhao and B. Z. Tang, *Adv. Opt. Mater.*, 2018, **6**, 1800264.
43 J. Huang, Z. Xu, Z. Cai, J. Guo, J. Guo, P. Shen, Z. Wang, Z. Zhao, D. Ma and B. Z. Tang, *J. Mater. Chem. C*, 2019, **7**, 330–339.
44 S. Song, P. Zhang, H. Liu, X. Zhu, X. Feng, Z. Zhao and B. Z. Tang, *Dyes Pigm.*, 2021, **196**, 109776.
45 Y.-J. Shiu, Y.-C. Cheng, W.-L. Tsai, C.-C. Wu, C.-T. Chao, C.-W. Lu, Y. Chi, Y.-T. Chen, S.-H. Liu and P.-T. Chou, *Angew. Chem., Int. Ed.*, 2016, **55**, 3017–3021.
46 J. Guo, J. Fan, L. Lin, J. Zeng, H. Liu, C.-K. Wang, Z. Zhao and B. Z. Tang, *Adv. Sci.*, 2019, **6**, 1801629.
47 C. Chen, H.-Y. Lu, Y.-F. Wang, M. Li, Y.-F. Shen and C.-F. Chen, *J. Mater. Chem. C*, 2019, **7**, 4673–4680.
48 K. Matsuo and T. Yasuda, *J. Mater. Chem. C*, 2019, **10**, 10687–10697.
49 X. Qiu, G. Tian, C. Lin, Y. Pan, X. Ye, B. Wang, D. Ma, D. Hu, Y. Luo and Y. Ma, *Adv. Opt. Mater.*, 2021, **9**, 2001845.
50 V. Thangaraji, P. Rajamalli, J. Jayakumar, M.-J. Huang, Y.-W. Chen and C.-H. Cheng, *ACS Appl. Mater. Interfaces*, 2019, **11**, 17128–17133.
51 K. Wang, C.-J. Zheng, W. Liu, K. Liang, Y.-Z. Shi, S.-L. Tao, C.-S. Lee, X.-M. Ou and X.-H. Zhang, *Adv. Mater.*, 2017, **29**, 1701476.

